

# A Topological Deep Learning Framework for Neural Spike Decoding

**Edward C. Mitchell**

Department of Mathematics  
University of Tennessee, Knoxville  
emitch39@vols.utk.edu

**Brittany Story**

National Institute for Mathematical and Biological Synthesis  
University of Tennessee, Knoxville

**David Boothe**

US Army Research Laboratory

**Piotr J. Franaszczuk**

US Army Research Laboratory and  
Department of Neurology  
Johns Hopkins University School of Medicine

**Vasileios Maroulas**

Department of Mathematics  
University of Tennessee, Knoxville  
vasileios.maroulas@utk.edu

## Abstract

The brain's spatial orientation system uses different neuron ensembles to aid in environment-based navigation. One of the ways brains encode spatial information is through grid cells, layers of decked neurons that overlay to provide environment-based navigation. These neurons fire in ensembles where several neurons fire at once to activate a single grid. We want to capture this firing structure and use it to decode grid cell data. Understanding, representing, and decoding these neural structures require models that encompass higher order connectivity than traditional graph-based models may provide. To that end, in this work, we develop a topological deep learning framework for neural spike train decoding. Our framework combines unsupervised simplicial complex discovery with the power of deep learning via a new architecture we develop herein called a simplicial convolutional recurrent neural network (SCRNN). Simplicial complexes, topological spaces that use not only vertices and edges but also higher-dimensional objects, naturally generalize graphs and capture more than just pairwise relationships. Additionally, this approach does not require prior knowledge of the neural activity beyond spike counts, which removes the need for similarity measurements. The effectiveness and versatility of the SCRNN is demonstrated on head direction data to test its performance and then applied to grid cell datasets with the task to automatically predict trajectories.

**Keywords:** simplicial complex, topological data analysis, grid cells, head direction cells, automated navigation

## 1 Introduction

Neurophysiological recording techniques have produced simultaneous recordings from increased numbers of neurons, both *in vitro* and *in vivo*, allowing for access to the activity of the hundreds of neurons required to encode certain variables [1, 2, 3, 4]. This makes efficient algorithms for decoding the information content from neural spike trains of increasing interest. Neural decoding can help provide insight into the function and significance of individual neurons or even entire regions of the brain [5]. Further, recent work in the area of brain-machine interfaces has integrated neural decoding of brain cells of certain utility into models used for prosthetic device control, perceptual readout, and communication with disabled patients [6, 7, 8]. One particular type of brain cell recently recorded in a quantity that allows for the analysis of its functional connectivity and structure of its population activity is the grid cell [1].

Grid cells are believed to be pivotal to mammalian navigation by playing a role in path integration [9, 10, 11], which is the integrating of one’s velocities, and vector-based navigation, the planning of trajectories to target locations [12, 13, 14]. Grid cells encode two-dimensional allocentric location by forming hexagonal, periodic firing fields within an environment [9, 10, 12]. Grid cells with firing fields exhibiting the same spacing and orientation form what are referred to as modules [10, 15]. Due to the critical role grid cells play in the mammalian navigation system, we are interested in decoding grid cell activity.

Decoding methods typically employ statistical or deep learning based models since one may view them as a regression problem where we learn the relationship between the dependent variable being decoded and the independent spike trains. Statistical methods like, but not limited to, linear regression, Bayesian reconstruction, and Kalman filtering are utilized for their interpretability and relatively low computational cost [16, 17, 18]. On the other hand, deep learning for neural decoding is a rapidly growing field due to neural networks’ observed success at time-series tasks like sequence prediction as well as neural networks’ ability to generalize beyond training data [18, 19, 20, 21]. Neural networks have outperformed statistical methods at decoding head direction and two-dimensional, environment-based position from neural recordings of head direction (HD) cells and place cells, respectively [18, 22, 23]. Deep learning’s superior decoding performance has been observed for a variety of network architectures including recurrent (RNNs) [24, 25], fully-connected feed forward (FFNNs), and convolutional neural networks (CNNs) [20, 26]. The smaller network sizes required for success in decoding compared to visual tasks allows for state-of-the-art performance on limited amounts of data [16]. Existing grid cell decoding efforts simulate grid cell activity within a heavily-tuned deep learning-based model trained on a spatial orientation or navigational task, and the simulated activity is then decoded using fully-connected feed forward or recurrent layers [27, 28]. However, these deep learning applications to neural decoding utilize architectures that ignore the underlying structure of the input neural activity.

Neurons in the brain form dense connections that lead to heavily correlated activity. Beyond these structural connections, higher-dimensional functional connectivity has been observed within groups of neurons exhibiting similar firing properties; for example, grid cells within a module [9]. Simplicial complexes, topological spaces with the ability to describe multi-way relationships, naturally lend themselves to defining and encapsulating the hierarchical properties of neuronal data [9, 29], making them an increasingly popular tool for representing neural activity [1, 30, 31, 32, 33, 34].

We propose a topological deep learning framework for neural spike train decoding by defining population activity on a simplicial complex that is then embedded in our new neural network architecture called a *simplicial convolutional recurrent neural network* (SCRNN), see Figure 1. The neural activity is defined on a simplicial complex via a pre-processing procedure, see Figure 4, which consists of binning the spikes to generate a spike count matrix that is then binarized, and active cells within a time bin are connected by a simplex. The construction of the simplicial complex makes no assumptions about the spike train’s encoding, and the higher dimensional connectivity of the simplicial complex ameliorates feature representation. Note the pre-processing procedure does not require prior knowledge of the neural activity beyond spike counts, thus avoiding the high computational cost of computing properties such as wavelet representations, coactivity, or other similarity measurements. The SCRNN employs simplicial convolutional layers [35, 36, 37, 38], see Figure 5, to extract features from the simplicial complex that are then fed to recurrent layers.

We first validate the method by decoding head direction from a population of HD cells, and compare the results to those produced by other neural network (NN) architectures. Next, we demonstrate the effectiveness of the method by decoding two-dimensional location from a population of grid cells. Notably, to the best of our knowledge, our grid cell decoding task marks one of the first deep learning applications to decoding experimental grid cell data. Most difficulties accompanying decoding experimental, rather than simulated, neuronal data can be attributed to the inherent noise in the data itself as well as the number of cells required to encode certain variables. This noise may be typically generated from recording devices and the fact that some cells are responsible for encoding more than one piece of information [10]. Several steps of the pre-processing procedure were designed with such noise in mind (details in Discussion, Section 3 and Methods, Section 4).

A summary of this paper’s contributions are listed below.

- First deep learning decoding of experimental grid cell data
- Develop a novel neural network architecture suited for sequenced data with irregular connectivity
- Improve feature extraction of neural data by defining neural activity on a simplicial complex and extracting features via simplicial convolutions

The paper is organized as follows. In Section 2, we provide a comparison of our framework to existing NN architectures by decoding HD data. In addition, we perform the more complex task of decoding location from three modules of grid cells. In Section 3, we elaborate on our results and outline potential future uses of the framework. Finally, in Section 4

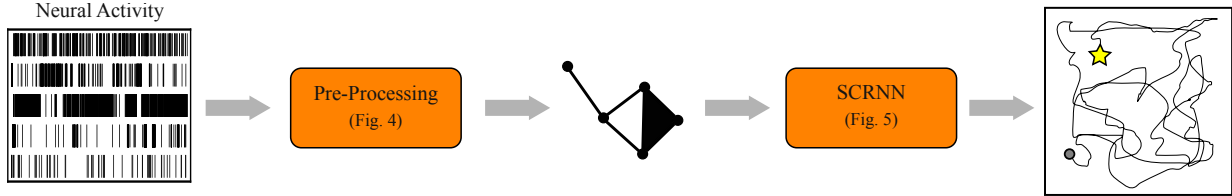


Figure 1: An overview of our framework. Neural data in the form of spike trains, represented by a raster plot, is defined on a simplicial complex via a pre-processing procedure, see Figure 4. The raster shown includes the activity of only five neurons for clarity. The simplicial complex gets input into a SCRNN, see Figure 5. Finally, the SCRNN decodes the desired variable(s). Here, we depict 2D location being decoded with the start and end locations of the trajectory depicted by a circle and star, respectively.

discusses details about the data used and provides specifics on the pre-processing procedure as well as the architecture of the SCRNN.

## 2 Results

The goal of a simplicial convolutional layer is to improve feature extraction by enforcing interpretable connectivity on the data, thus creating meaningful information sharing. The simplicial convolutional layers achieve this by considering a simplicial complex and applying an information-sharing operator generated by the connectivity of the embedded simplicial complex (details in Methods, Section 4). The motivating intuition behind employing the recurrently connected layers is their proven ability to handle sequenced data better than fully connected layers. This intuition is empirically validated below on experimental HD data.

To define the population activity of a group of cells on a simplicial complex, we partition time into non-intersecting bins and compute the spike counts for each bin. After a thresholding procedure, active cells within a time bin are connected via the appropriate-dimensional simplex. The result is a simplicial complex where connectivity is generated by functional activity. That is, simplices do not represent anatomically supported structural connections between neurons, but rather a temporally linked firing of neurons. For additional information, see Figure 4. We call this complex the *functional simplicial complex*.

For comparison of the SCRNN to existing NN architectures, we decode experimental HD data using an FFNN and an RNN. To highlight the role of the recurrent layers of the SCRNN, we also employ an architecture consisting of simplicial convolutional layers attached to fully connected feed-forward layers; we refer to this network as the *simplicial convolutional neural network* (SCNN).

Finally, after testing all four methods on the HD data and demonstrating that the SCRNN has the best performance, we implement our SCRNN framework on the more complex task of decoding three modules of grid cells that includes conjunctive grid/HD cells. Below, we outline the results for both the head direction and grid cell tasks.

**Head Direction Cells.** The neurons making up the head direction (HD) system in the brain encode the direction the head is facing at any given time. This encoding is done by identifying different ensembles of certain neurons, called HD cells, which fire simultaneously, where each grouping of cells represents a different direction [39]. To demonstrate the effectiveness of our method, we analyze HD data recorded in [17]. This dataset contains the spike data of 22 neurons, and to reduce computational cost, we looked at the first 20 minutes of a 38 minute foraging session for a single mouse.

Decoding accuracy was measured in three different ways. First, we considered the median absolute error (MAE), which is defined,

$$MAE = \underset{n=1, 2, \dots, N_{time}}{\text{median}} | \text{rescale}[\theta_{dec}(n) - \theta_{true}(n)] | , \quad (1)$$

where  $N_{time}$  is the number of time bins, and  $\theta_{dec}$ ,  $\theta_{true} \in [0^\circ, 360^\circ]$  are the decoded and the ground truth directions, respectively. The mapping *rescale* accounts for the ring structure of HD. For example,  $310^\circ$  and  $20^\circ$  should be recorded as a difference of  $70^\circ$  instead of  $290^\circ$ .

Similarly, we compute the average absolute error (AAE), which considers the average instead of the median discrepancy as defined below,

$$AAE = \frac{1}{N_{time}} \sum_{n=1}^{N_{time}} |rescale[\theta_{dec}(n) - \theta_{true}(n)]| . \quad (2)$$

The final recorded error is the catastrophic error, denoted as CAT, which counts the number of predictions off by  $90^\circ$  or more from the real HD, since this would imply that our prediction is completely wrong. We focus on CAT error based on the importance of bounding the cost of a single error as opposed to just bounding the overall error [40]. That is, considering the median or average of errors places less significance on the larger outliers that can have devastating consequences in applications of models employing neural decoding.

We ran 10 trials with 75% of the data used for training and 25% of the data used for testing for each method using the hyperparameters listed in Supplementary Material Table 1. The FFNN recorded MAE = 12.75, AAE = 16.85 and CAT = 70, and the SCNN method recorded MAE = 11.56, AAE = 15.43, and CAT = 94. The RNN yielded MAE = 11.26, AAE = 14.49, and CAT = 9 whereas the SCRNN produced MAE = 10.96, AAE = 14.11, and CAT = 6. All around the SCRNN performed the best across all different architectures. Similarly, if we instead use 50% for training and 50% for testing or 25% minutes for training and 75% for testing, the SCRNN still outperforms the other three networks. See the Supplementary Material for additional tests and hyperparameter tuning information.

Thus, we conclude that inputting the underlying simplicial complex structure into the network and using its connectivity to generate information-sharing gives a lower MAE, AAE, and CAT error rate than traditional neural networks. With this in mind, we apply the SCRNN to grid cells; a different type of cell that encodes environment-based location.

**Grid Cells.** Layers in the Medial Entorhinal Cortex (MEC) have been shown to include both pure grid cells which are believed to fire independent of head direction and conjunctive grid/HD cells which display firing patterns tuned to a single head direction [1, 41]. We decode the position (as in xy-coordinates) from the activity of a population of cells recorded in a moving rat, which contains pure grid cells and conjunctive grid/HD cells [1].

Due to the fact firing fields for cells within a module are the same, except for a shift in space, it takes more than one module to encode position [15, 42]. Cells firing at the same time within a module generate a spatial grid over the environment. A multi-scale representation for location is then created by layering the grids generated by different modules. In the following analysis, we look at a population of 482 cells that contains three grid modules consisting of 166, 167, and 149 cells total with 93, 149, and 145 of them being pure grid cells, respectively; for a look at the spike trains from the first module, see Supplementary Material Figure 9. The rest of the population is made up of conjunctive grid/HD cells. The difficulties of decoding such a population stem from not only the large amount of cells, but also the fact that some cells are not solely responsible for encoding position, the target variable we aim to decode [10]. The larger population of cells and, consequently, the larger size of the functional simplicial complex compared to the HD decoding task, means a more heavily parameterized SCRNN is required to decode position.

To measure the success of our model, we compute the Average Euclidean Distance (AED) across all time-bins:

$$AED = \frac{1}{N_{time}} \sum_{n=1}^{N_{time}} \sqrt{(x_{dec}(n) - x_{true}(n))^2 + (y_{dec}(n) - y_{true}(n))^2} , \quad (3)$$

where  $N_{time}$  is the number of time bins,  $(x_{dec}, y_{dec})$  are the decoded xy-coordinates, and  $(x_{true}, y_{true})$  are the ground-truth xy-coordinates.

We tuned hyperparameters to minimize AED. With the hyperparameters detailed in Supplementary Material, we calculate the AED from Equation (3) on the training and test data with an 80% training and 20% testing split. We find our model is able to achieve an AED = 0.0286 meters (m) on the training data and AED = 0.1473m on the test data. Thus, the SCRNN is clearly able to learn the pattern between grid cell activity and position in the environment. A discrepancy between training and test results is expected given the fact grid cells may not encode the exact location, so training could bias the network to map neural codes for general locations to the specific labelled locations included in the training data.

### 3 Discussion

Notably, the simplicial convolutional framework was able to successfully decode a population containing pure grid and conjunctive grid/HD cells. Decoding position from the activity of a population containing more than just pure grid cells

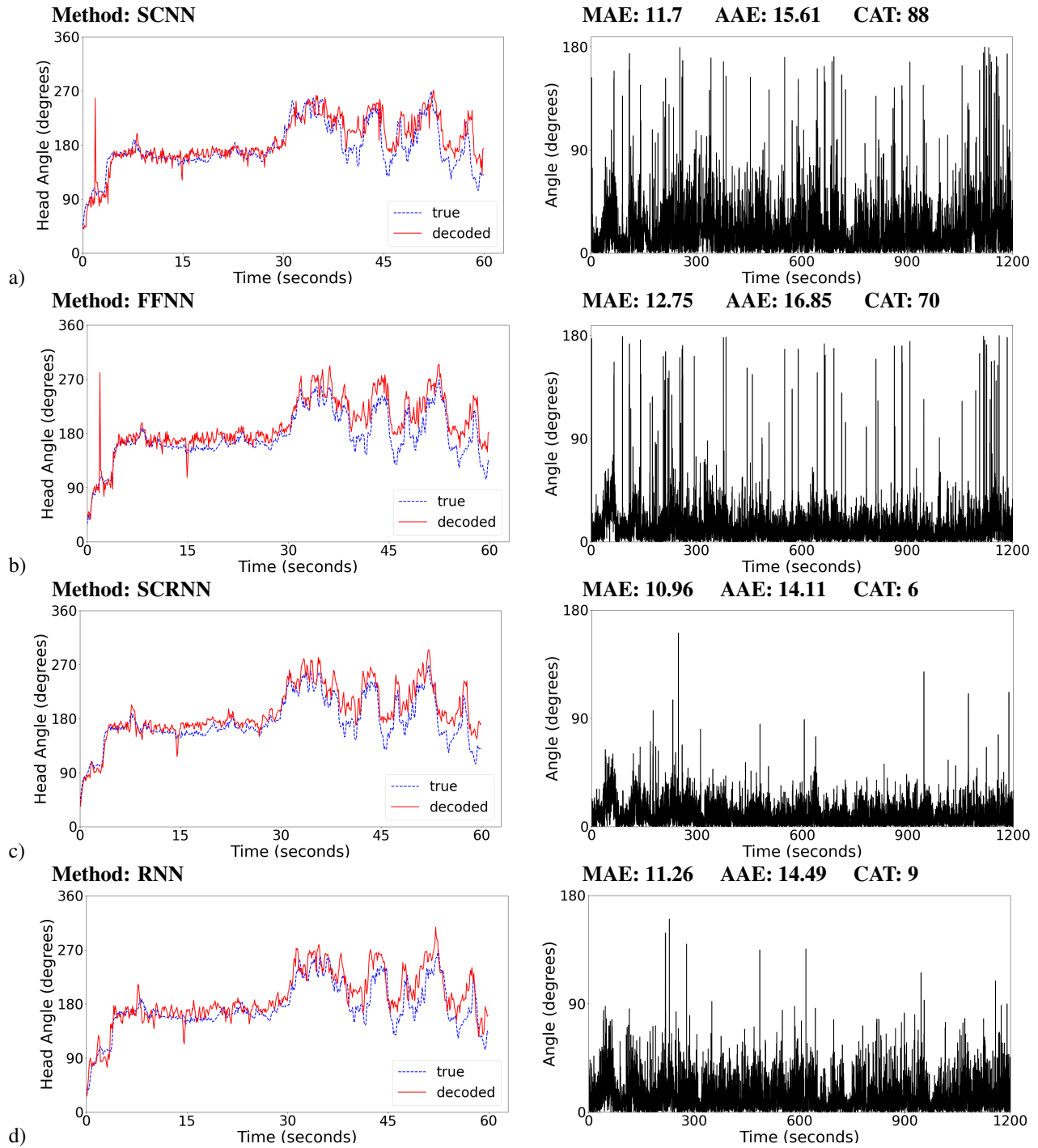


Figure 2: Plots depicting the true head angle and the predicted head angle for the first two minutes (left) and the catastrophic error for each time bin for the full twenty minutes (right) for four different networks, a) SCNN, b) FFNN, c) SCRNN, and d) RNN.

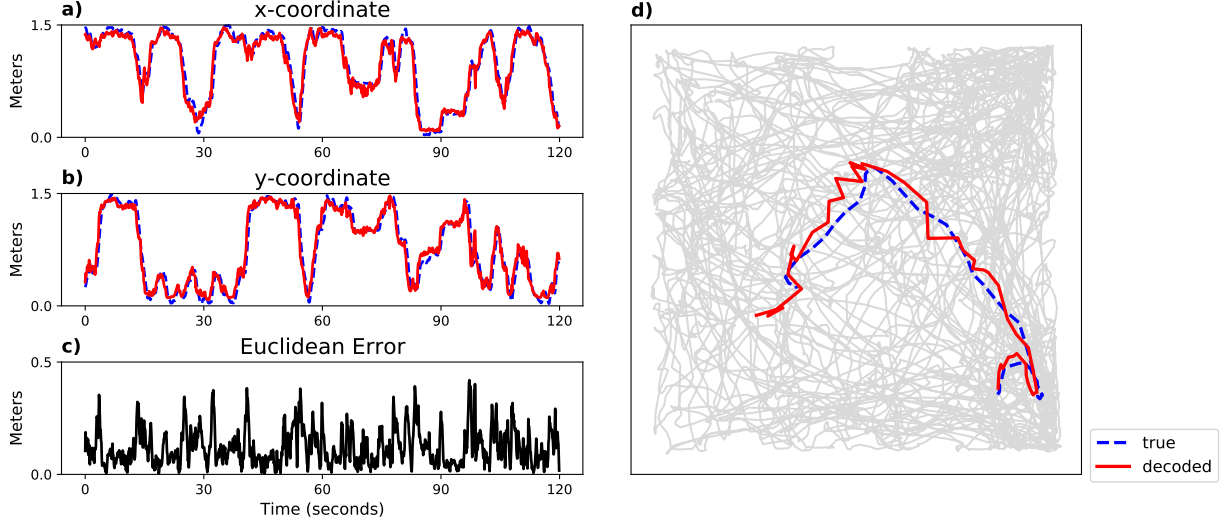


Figure 3: a-c) Plots showing results from two minutes of the grid cell decoding task. a) Comparison of decoded versus ground truth x–coordinate. b) Comparison of decoded versus ground truth y–coordinate. c) Error for each time bin measured by equation (3). d) In grey is the ground truth position of the rat in the environment for all time bins used. Though we decode the entire trajectory shown in grey, for visual purposes, we include colorized paths showing a 5 second comparison of decoded versus ground truth position.

requires a framework robust to noisy input data, which our pre-processing is heuristically designed to be by binning spike counts and thresholding out low-activity time windows for each neuron.

The results also showed defining neural activity on a simplicial complex and extracting features via simplicial convolutions that are then fed to recurrent layers improves the decoding of HD cell spike train data. It is not surprising that the SCRNN provided better results than the FFNN and SCNN, which lack recurrent connections, considering the time-series nature of the data. Further, the recurrent layers in the back-end RNN are more biologically relevant than those of an FFNN: the hidden states in the recurrent layers act as memory buffers similar to the working memory maintained within the prefrontal cortex in human brains [43].

This work features a low-complexity version of the framework to assist with network comparison and reducing computation time. For comparison purposes, the number of deep learning techniques applied to any NN architecture was kept to a minimum: only dropout, which itself was inspired by the stochastic Poisson-like firing of neurons [43, 44], was employed. For computational purposes, the maximal simplicial dimension was capped at two. Future work could involve higher complexity, for example, a biologically relevant functional simplicial complex of higher dimensions where simplices imply a connection that is experimentally supported. In both the low-complexity and biologically inspired cases, it would be worthwhile to analyze the learned filter parameters and better understand the dynamics of the simplicial convolutional layers. Similar analysis to existing NN architectures, such as CNNs, has shown an understanding of the learned parameter space can be exploited to improve network performance [45].

Further analysis of the simplicial convolutional layers of a successfully trained decoding model could help with understanding the dynamics of the decoded population. Specific to the grid cell application, layers simulating grid cell activity within a path navigation model could employ a simplicial encoder [35] and simplicial convolutional layers. The encoder would generate simplicial complex representations of space that are then decoded using the simplicial convolutions. This would differ from existing deep learning-based navigational models [27, 28] in that it would take into account the functional connectivity in both the encoding and decoding of spatial location.

Though this work focused on decoding population activity from single cell recordings, the simplicial convolutional framework has wider applicability. With only slight modifications, the framework can be adapted to other computational neuroscience tasks like brain-machine interfaces [46] or epileptic seizure detection [47], essentially any task where connectivity and higher dimensional relationships have traditionally been ignored. Beyond the scope of neuroscience, the SCRNN can be used on any dataset where shape can be characterized by a simplicial complex. A recent increase in works employing tools from Topological Data Analysis (TDA) has revealed that the underlying shape of data can be exploited to improve performance in tasks across a number of domains [48, 49, 50].

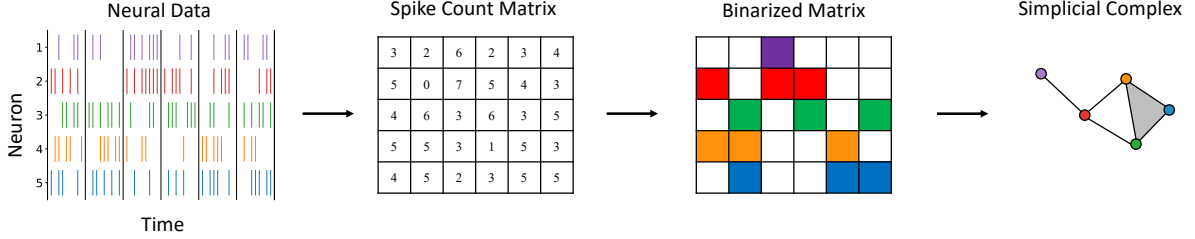


Figure 4: An example of the pre-processing procedure. Neural spiking data is represented as a raster plot on the left. The data is binned and converted to a spike count matrix. A row-wise thresholding procedure, given in Equation (4), binarizes the matrix. The binary matrix is displayed here with elements equal to 1 being colored in and the white elements conveying a 0. The colored regions within each column are then connected via the appropriate dimensional simplex to create the simplicial complex. For example, we see that the second column of the binarized matrix has three active neurons (green, orange, and blue). This generates a 2-simplex on the corresponding nodes. Note this allows for a multi-way description of these three nodes' relationship as opposed to the clique of 1-simplices that can only describe these nodes by their pairwise relationships.

## 4 Methods

**HD data.** Here we provide a short summary of the HD data recorded in [17]. The spike times of HD cells in the anterodorsal thalamic nucleus (ADn) along with the corresponding ground truth head angles of seven mice were recorded using multi-site silicon probes and an alignment of LED lights on the mice's headstage, respectively. The sessions recorded comprised of two hours of sleep followed by 30-45 minutes of foraging in an open rectangular environment followed by 2 more hours of sleep. For the results shown in this work, we used the foraging portion of session 'Mouse28-140313' in [17].

**Grid cell data.** What follows is a brief description of the grid cell data reported in [1]. Neural activity was recorded in layers II and III of the medial entorhinal cortex using high-site-count Neuropixels silicon probes [3, 4] while rats foraged alone in an open square  $1.5\text{m} \times 1.5\text{m}$  arena. Three-dimensional motion capture was utilized to track the rats' head directions and two-dimensional positions in the environment. The results presented in this paper use modules labeled R1-R3 day one in the source data [1].

**Pre-processing.** The experimental HD data and grid cell data consist of neurons and their corresponding spike times. Given the spike times of  $N$  simultaneously recorded neurons, we first construct a spike count matrix  $A$  by creating  $N_{\text{time}}$  non-intersecting bins of width  $t_{\text{bin}}$  and counting each individual neuron's number of spikes within each bin, shown in Figure 4. The element  $A_{ij}$  is then set equal to the spike count of neuron  $i$  within bin  $j$ . The next step is to binarize  $A$  via a row-wise thresholding procedure. For a fixed row, consider the elements  $\{a_\ell\}_{\ell=1}^{N_{\text{time}}}$  ordered from highest to lowest. Then for some value  $p \in (0, 1]$ , we select  $\{a_\ell\}_{\ell=1}^{m^*}$  for  $m^*$  given by,

$$m^* = \arg \min_{1 \leq m \leq N_{\text{time}}} \left\{ \sum_{\ell=1}^m a_\ell \text{ s.t. } \sum_{\ell=1}^m a_\ell \geq p \cdot \sum_{\ell=1}^{N_{\text{time}}} a_\ell \right\}. \quad (4)$$

The  $m^*$  selected row elements are then set to 1 while the remaining  $N_{\text{time}} - m^*$  elements are set to 0. This is repeated for every row of  $A$  using the same value for  $p$  as before. Note that thresholding row-wise accounts for the variability in total spikes among neurons by comparing each neuron's activity against itself. We then proceed column-wise through the binarized matrix, connecting each active neuron within a time bin by the appropriate-dimensional simplex, see Figure 4. Specifically, if there are  $0 \leq n_{\text{act}} \leq N$  active neurons in a column, an  $(n_{\text{act}} - 1)$ -simplex is constructed on the nodes corresponding to those  $n_{\text{act}}$  rows.

**Simplicial complexes.** We introduce simplices and simplicial complexes, the topological structures we exploit for feature representation. For more information on simplicial complexes, see [51].

**Definition 1.** A collection  $\{v_0, v_1, \dots, v_n\} \subset \mathbb{R}^d \setminus \{0\}$  is *geometrically independent* if and only if for any  $\{t_0, t_1, \dots, t_n\} \subset \mathbb{R}$  with  $\sum_{i=0}^n t_i = 0$ , the condition  $\sum_{i=0}^n t_i v_i = 0$  implies  $t_i = 0$  for all  $i \in \{0, 1, \dots, n\}$ .

**Definition 2.** A  $k$ -simplex,  $s^k$ , is the convex hull of  $k + 1$  geometrically independent points  $\{v_0, v_1, \dots, v_k\}$ , denoted by  $[v_0, v_1, \dots, v_k]$ .

**Definition 3.** The *faces* of a  $k$ –simplex  $[v_0, v_1, \dots, v_k]$  are the  $(k-1)$ –simplices given by  $[v_0, \dots, v_{j-1}, v_{j+1}, \dots, v_k]$  for some  $j \in \{0, 1, \dots, k\}$  and are denoted  $s_j^{k-1} \subset s^k$ .

**Definition 4.** A *simplicial complex*  $S$  is a collection of simplices satisfying

1. if  $s \in S$ , then every face of  $s$  is in  $S$  and
2. if  $s_1, s_2 \in S$ , then  $s_1 \cap s_2 = \emptyset$  or  $s_1 \cap s_2 \in S$ .

To ease understanding, one may consider a 0-simplex as a vertex, a 1-simplex as an edge, a 2-simplex as a triangle, a 3-simplex as a tetrahedron, and so on. Orientation can be assigned to  $k$ –simplices forming what is called an *ordered  $k$ –simplex*. For a face  $s_j^{k-1} \subset s^k$ , if the orientation of  $s_j^{k-1}$  coincides with that of  $s^k$ , we write  $s_j^{k-1} \prec s^k$ . Additionally, features, typically vectors or scalars, can also be assigned to the simplices. The features of the  $k$ –simplices are represented by a vector, or matrix depending on the feature size, called the  *$k$ –cochain*, and it is denoted by  $c_k$ .

**Definition 5.** Let  $\{s_i^k\}_{i=1}^{N_k}$  be the ordered  $k$ –simplices of a simplicial complex. Then for each  $s_i^k \in \{s_i^k\}_{i=1}^{N_k}$ , assign a feature  $c^i \in \mathbb{R}^{N_{feat}}$ . The  *$k$ –cochain*,  $c_k \in \mathbb{R}^{N_k \times N_{feat}}$ , is then given,

$$[c_k]_{ij} = [c^i]_j. \quad (5)$$

**Simplicial convolutional recurrent neural network.** It is common practice for neural activity to be converted to a matrix where rows represent individual neurons and columns correspond to time bins. The most widely used deep learning approach to handling matrices as inputs is to employ a convolutional neural network (CNN). In a CNN, convolutional layers extract features from the input by aggregating weighted information from neighboring elements in the input matrix. This localization of information-sharing assumes regular connectivity where only neighboring rows, or columns, possess significance to each other. Thus, in tasks where rows of a matrix neighboring each other bares no significance, CNNs do not intuitively extract features.

Simplicial convolutions generalize convolutions to account for data with irregular connectivity. For these layers, input data is defined on a simplicial complex, and information-sharing is generated by the *Hodge-Laplacian*. To define the Hodge-Laplacian, we must first introduce the  *$k$ –dimensional incidence matrix*,  $B_k \in \mathbb{R}^{N_{k-1} \times N_k}$ , where the  $ij$ th element is given by,

$$[B_k]_{ij} = \begin{cases} 0, & \text{if } s_i^{k-1} \not\subset s_j^k, \\ -1, & \text{if } s_i^{k-1} \subset s_j^k \text{ and } s_i^{k-1} \not\prec s_j^k, \\ 1, & \text{if } s_i^{k-1} \subset s_j^k \text{ and } s_i^{k-1} \prec s_j^k, \end{cases} \quad (6)$$

where  $N_{k-1}$  and  $N_k$  are the number of  $(k-1)$ –simplices and  $k$ –simplices, respectively. Note, we consider  $B_0 = 0 \in \mathbb{R}^{N_0 \times N_0}$ . Then, finally, the  *$k$ –Hodge-Laplacian*,  $L_k \in \mathbb{R}^{N_k \times N_k}$ , is defined as,

$$L_k = B_k^T B_k + B_{k+1} B_{k+1}^T. \quad (7)$$

In simplicial convolutions, the terms of the Hodge-Laplacian in equation (7) act as shift-operators defining which simplices of the same dimension share information. The terms  $B_k^T B_k$  and  $B_{k+1} B_{k+1}^T$  are called the *lower* and *upper Laplacian*, and they capture connectivity by lower and higher dimensional simplices, respectively. A *degree  $D$  simplicial filter* consisting of weights  $W = \{W_i\}_{i=0}^{2D}$  is an operator,  $H_k \in \mathbb{R}^{N_k \times N_k}$ , given by,

$$H_k = W_0 I + \sum_{i=1}^D W_i (B_k^T B_k)^i + \sum_{i=1}^D W_{i+D} (B_{k+1} B_{k+1}^T)^i, \quad (8)$$

where  $k$  is the dimension of simplices and  $(\cdot)^i$  denotes the  $i$ –th power of a matrix. Note, each power of the lower and upper Laplacians localizes information-sharing to within the  $i$  nearest  $k$ –simplices, similar to increasing the filter size in a traditional convolutional layer.

We now discuss the dynamics of the *simplicial convolutional layers* of an SCRNN. The proof of the following proposition is delegated to the Supplementary Materials.

**Proposition 1.** Consider an SCRNN consisting of  $L$  simplicial convolutional layers, each equipped with  $F$  filters,  $\{H_k^f(\ell)\}_{f=1}^F$ , for each dimension  $k$  of the functional simplicial complex with maximum simplicial dimension  $K$ , where  $\ell \in \{1, 2, \dots, L\}$  denotes the simplicial convolutional layer. In such a network, the number of parameters used in the simplicial convolutional layers is  $F[2(D+1) + (K-1)(2D+1)]L$ .

Note that the dynamics of the simplicial convolutional layers prevent exponential growth of parameters with respect to filters and number of layers.

For the first layer  $\ell = 1$ , features  $\{\mathbf{x}_k^f(1)\}_{f=1}^F$  are extracted from the input,  $\mathbf{x}_k(0)$ , via the nonlinear transformations,

$$\mathbf{x}_k^f(1) = \sigma \left( H_k^f(1) \mathbf{x}_k(0) \right), \quad (9)$$

for each  $f = 1, 2, \dots, F$  and  $k = 1, 2, \dots, K$ . Note  $\mathbf{x}_0(0) \in \mathbb{R}^{N_0 \times n_{col}}$  for some hyperparameter  $1 \leq n_{col} \leq N_{time}$ , and  $\mathbf{x}_k(0) \in \mathbb{R}^{N_k}$  for  $1 \leq k \leq K$ . For the intermediate simplicial convolutional layers  $\ell = 2, 3, \dots, L-1$  and fixed  $k$ , each of the filters  $\{H_k^f(\ell)\}$  is applied to each of the extracted features from the previous layer. To prevent the exponential growth of the number of filters, the outputs extracted from the same feature from the previous layer are summed together to create one single output feature. That is, for each feature  $\{\mathbf{x}_k^g(\ell-1)\}_{g=1}^F$  from the previous layer, we extract,

$$\mathbf{x}_k^g(\ell) = \sigma \left( \sum_{f=1}^F H_k^f(\ell) \mathbf{x}_k^g(\ell-1) \right), \quad (10)$$

for  $g \in \{1, 2, \dots, F\}$ . In the final simplicial convolutional layer,  $\ell = L$ , features are extracted following the same procedure as the intermediate layers, but additionally, all extracted features are summed:

$$\mathbf{x}_k(L) = \sum_{g=1}^F \mathbf{x}_k^g(L) = \sum_{g=1}^F \sigma \left( \sum_{f=1}^F H_k^f(\ell) \mathbf{x}_k^g(\ell-1) \right), \quad (11)$$

where  $\mathbf{x}_k^g(L)$  as in Equation (10) for  $\ell = L$ . If  $1 < n_{col}$ , then  $\mathbf{x}_0(L)$  is summed across columns, which gives us  $\mathbf{x}_0(L) \in \mathbb{R}^{N_0}$ . Finally, the outputs for each dimension of the simplicial complex,  $\{\mathbf{x}_k(L)\}_{k=1}^K$ , are stacked to create one output feature vector,  $\mathbf{x}(L) \in \mathbb{R}^{\sum_{k=0}^K N_k}$ . For illustrative purposes, Figure 5, depicts  $L = 2$  simplicial convolutional layers each consisting of  $F = 3$  filters for each dimension of the input simplicial complex.

To form an input sequence to the RNN component of the SCRNN, we consider the outputs of the simplicial convolutional layers corresponding to a desired number of consecutive time bins. Given the sequential nature of the decoding task, we append the simplicial convolutional layers with a multi-layer RNN, a neural network architecture designed for time-series data. We opt for the Elman RNN architecture [24] over its more complex counterpart, the long short-term memory network (LSTM) [52], because only neural activity recorded in time bins close to the target time bin bare any relevance to the decoded variable, thus, making the extra parameters in an LSTM designed for handling long sequences unnecessary. Elman RNNs utilize what are called hidden states to handle sequential data. For each input,  $\mathbf{x}_t$ , we compute a hidden state,  $h_t$ , from the input sequence, given by,

$$h_t = \sigma (W_h \mathbf{x}_t + b_h + W_c h_{t-1} + b_c), \quad (12)$$

where  $W_h, W_c$  are weight matrices and  $b_h, b_c$  are bias vectors. The final output of an RNN is obtained by computing the nonlinear mapping of a linear transformation of the hidden state; that is,

$$y_t = \sigma (W h_t + b), \quad (13)$$

where  $h_t$  as in Equation (12). Finally, a multi-layer RNN is created by stacking multiple RNNs, feeding the outputs of one as the inputs to another.

**SCRNN input.** Sub-complexes corresponding to a desired number,  $n_{col}$ , of consecutive time bins (columns of the spike count matrix  $A$ ) are used as inputs to the SC layers. Suppose we aim to find the value of the decoded variable in time bin  $n_t$ , where  $n_{col} \leq n_t \leq N_{time}$ . Then the elements of the 0-cochain,  $c_0(n_t) \in \mathbb{R}^{N_0 \times n_{col}}$ , are given

$$[c_0(n_t)]_{ij} = [A]_{i(n_t - n_{col} + j)}, \quad (14)$$

for  $i = 1, 2, \dots, N$  and  $j = 1, 2, \dots, n_{col}$ . The 1-cochains are the Pearson product-moment correlation coefficients of the row-vectors of  $A$  corresponding to the 1-simplices' faces. Let  $N_1$  denote the number of 1-simplices present in the functional simplicial complex. After arbitrarily indexing the 1-simplices, let  $q(i)$  and  $r(i)$  denote the row index corresponding to the faces of the  $i$ th 1-simplex. We define the elements of the 1-cochain,  $c_1(n_t) \in \mathbb{R}^{N_1}$ , as follows: for any  $i \in \{1, 2, \dots, N_1\}$  not present in the  $n_t$  time bin, we set  $[c_1(n_t)]_i = 0$ ; otherwise,

$$[c_1(n_t)]_i = R_{q(i)r(i)}, \quad (15)$$

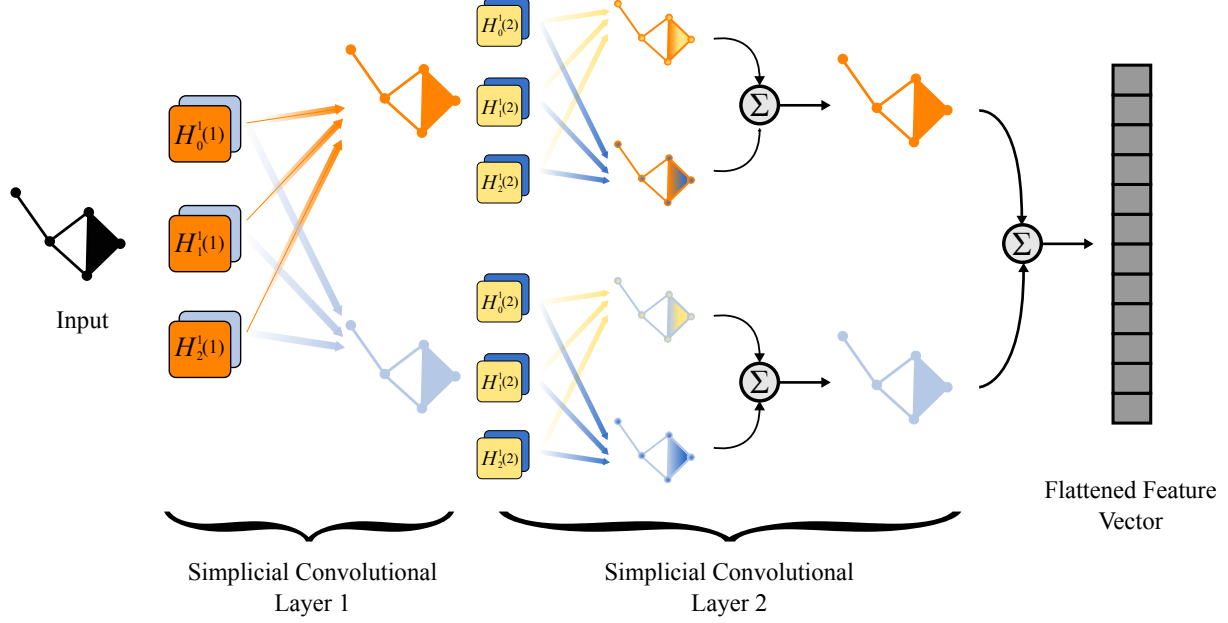


Figure 5: A diagram of  $L = 2$  simplicial convolutional layers each equipped with two filters,  $H_k^1(1)$  and  $H_k^2(1)$ , for each simplicial dimension  $k = 0, 1, 2$ . Filters are color coded with filters that get concatenated bearing the same color as the resultant simplicial complex. In the first layer, we see three orange filters indicating the three dimensions of the input simplicial complex. The features extracted using these filters result in a new, orange simplicial complex. The second filter, depicted in light blue, extracts a separate simplicial complex. In the second simplicial convolutional layer, the process is repeated with two new filters, depicted by yellow and dark blue. In order to prevent exponential growth, features extracted from the same input from the previous layer are summed. Finally, all extracted features are summed and flattened to create one feature vector.

where  $R_{q(i)r(i)}$  is the Pearson product-moment correlation coefficients of the  $q(i)$ th and  $r(i)$ th row-vectors of  $A$ . Similarly, for the 2-cochains, let  $q(i), r(i)$ , and  $u(i)$  denote the row index corresponding to the 0-simplices contained in the  $i$ th 2-simplex. We define the elements of the 2-cochain,  $c_2(n_t) \in \mathbb{R}^{N_2}$ , as follows: for any  $i \in \{1, 2, \dots, N_2\}$  not present in the  $n_t$  time bin, we set  $[c_2(n_t)]_i = 0$ ; otherwise,

$$[c_2(n_t)]_i = \min\{R_{q(i),r(i)u(i)}, R_{r(i),q(i)u(i)}, R_{u(i),q(i)r(i)}\}, \quad (16)$$

where  $R_{q(i),r(i)u(i)}$  denotes the multiple correlation coefficient of the  $q(i), r(i)$ , and  $u(i)$ th row-vectors of  $A$  with  $r(i)$  and  $u(i)$  considered dependent on  $q(i)$ . Higher dimensional cochains can be defined in a similar manner, but with a metric other than the correlation of the simplices' faces that can be chosen specific to the cell population being decoded.

**Code availability.** The code is available upon request.

**Acknowledgment.** This work has been partially funded by the US Army Research Lab Contract No W911NF2120186.

## References

- [1] Richard J. Gardner, Erik Hermansen, Marius Pachitariu, Yoram Burak, Nils A. Baas, Benjamin A. Dunn, May-Britt Moser, and Edvard I. Moser. Toroidal topology of population activity in grid cells. *Nature*, 602(7895):123–128, 2022.
- [2] Takashi Yoshida and Kenichi Ohki. Natural images are reliably represented by sparse and variable populations of neurons in visual cortex. *Nature Communications*, 11(1):872, 2020.
- [3] James J. Jun, Nicholas A. Steinmetz, Joshua H. Siegle, Daniel J. Denman, Marius Bauza, Brian Barbarits, Albert K. Lee, Costas A. Anastassiou, Alexandru Andrei, Çağatay Aydin, Mladen Barbic, Timothy J. Blanche, Vincent Bonin, João Couto, Barundeb Dutta, Sergey L. Gratiy, Diego A. Gutnisky, Michael Häusser, Bill Karsh, Peter Ledochowitsch, Carolina Mora Lopez, Catalin Mitelut, Silke Musa, Michael Okun, Marius Pachitariu, Jan Putzeys, P. Dylan Rich, Cyrille Rossant, Wei-lung Sun, Karel Svoboda, Matteo Carandini, Kenneth D. Harris, Christof Koch, John O’Keefe, and Timothy D. Harris. Fully integrated silicon probes for high-density recording of neural activity. *Nature*, 551(7679):232–236, 2017.
- [4] Nicholas A. Steinmetz, Cagatay Aydin, Anna Lebedeva, Michael Okun, Marius Pachitariu, Marius Bauza, Maxime Beau, Jai Bhagat, Claudia Böhm, Martijn Broux, Susu Chen, Jennifer Colonell, Richard J. Gardner, Bill Karsh, Fabian Kloosterman, Dimitar Kostadinov, Carolina Mora-Lopez, John O’Callaghan, Junchol Park, Jan Putzeys, Britton Sauerbrei, Rik J. J. van Daal, Abraham Z. Volland, Shiwei Wang, Marleen Welkenhuysen, Zhiwen Ye, Joshua T. Dudman, Barundeb Dutta, Adam W. Hantman, Kenneth D. Harris, Albert K. Lee, Edvard I. Moser, John O’Keefe, Alfonso Renart, Karel Svoboda, Michael Häusser, Sebastian Haesler, Matteo Carandini, and Timothy D. Harris. Neuropixels 2.0: A miniaturized high-density probe for stable, long-term brain recordings. *Science*, 372(6539):eabf4588, 2021.
- [5] Joshua I. Glaser, Ari S. Benjamin, Roozbeh Farhoodi, and Konrad P. Kording. The roles of supervised machine learning in systems neuroscience. *Prog Neurobiol*, 175:126–137, 04 2019.
- [6] Jonathan R. Wolpaw, Niels Birbaumer, Dennis J. McFarland, Gert Pfurtscheller, and Theresa M. Vaughan. Brain computer interfaces for communication and control. *Clinical Neurophysiology*, 113(6):767–791, 2002.
- [7] Xiang Zhang, Lina Yao, Xianzhi Wang, Jessica Monaghan, David Mcalpine, and Yu Zhang. A survey on deep learning-based non-invasive brain signals: recent advances and new frontiers. *J Neural Eng*, 18(3), 03 2021.
- [8] Michael A. Schwemmer, Nicholas D. Skomrock, Per B. Sederberg, Jordyn E. Ting, Gaurav Sharma, Marcia A. Bockbrader, and David A. Friedenberg. Meeting brain–computer interface user performance expectations using a deep neural network decoding framework. *Nature Medicine*, 24(11):1669–1676, 2018.
- [9] Torkel Hafting, Marianne Fyhn, Sturla Molden, May-Britt Moser, and Edvard I. Moser. Microstructure of a spatial map in the entorhinal cortex. *Nature*, 436(7052):801–806, 2005.
- [10] Bruce L. McNaughton, Francesco P. Battaglia, Ole Jensen, Edvard I Moser, and May-Britt Moser. Path integration and the neural basis of the ‘cognitive map’. *Nature Reviews Neuroscience*, 7(8):663–678, 2006.
- [11] Caitlin S. Mallory and Lisa M. Giocomo. From entorhinal neural codes to navigation. *Nature Neuroscience*, 21(1):7–8, 2018.
- [12] Ila R. Fiete, Yoram Burak, and Ted Brookings. What grid cells convey about rat location. *Journal of Neuroscience*, 28(27):6858–6871, 2008.
- [13] Daniel Bush, Caswell Barry, Daniel Manson, and Neil Burgess. Using Grid Cells for Navigation. *Neuron*, 87(3):507–520, Aug 2015.
- [14] Nils Nyberg, Éléonore Duvalle, Caswell Barry, and Hugo J. Spiers. Spatial goal coding in the hippocampal formation. *Neuron*, 110(3):394–422, 2022.
- [15] Alexander Mathis, Andreas V. M. Herz, and Martin Stemmler. Optimal Population Codes for Space: Grid Cells Outperform Place Cells. *Neural Computation*, 24(9):2280–2317, 09 2012.
- [16] Joshua I. Glaser, Ari S. Benjamin, Raeed H. Chowdhury, Matthew G. Perich, Lee E. Miller, and Konrad P. Kording. Machine learning for neural decoding. *eNeuro*, 7(4), 2020.
- [17] Adrien Peyrache, Marie M Lacroix, Peter C Petersen, and György Buzsáki. Internally organized mechanisms of the head direction sense. *Nature Neuroscience*, 18(4):569–575, 2015.

[18] Zishen Xu, Wei Wu, Shawn S. Winter, Max L. Mehlman, William N. Butler, Christine M. Simmons, Ryan E. Harvey, Laura E. Berkowitz, Yang Chen, Jeffrey S. Taube, Aaron A. Wilber, and Benjamin J. Clark. A comparison of neural decoding methods and population coding across thalamo-cortical head direction cells. *Frontiers in Neural Circuits*, 13, 2019.

[19] Alex Krizhevsky, Ilya Sutskever, and Geoffrey E Hinton. Imagenet classification with deep convolutional neural networks. In F. Pereira, C.J. Burges, L. Bottou, and K.Q. Weinberger, editors, *Advances in Neural Information Processing Systems*, volume 25. Curran Associates, Inc., 2012.

[20] Yann LeCun, Yoshua Bengio, and Geoffrey Hinton. Deep learning. *Nature*, 521(7553):436–444, 2015.

[21] Péter Szabó and Péter Barthó. Decoding neurobiological spike trains using recurrent neural networks: a case study with electrophysiological auditory cortex recordings. *Neural Computing and Applications*, 34(4):3213–3221, 2022.

[22] Markus Frey, Sander Tanni, Catherine Perrodin, Alice O’Leary, Matthias Nau, Jack Kelly, Andrea Banino, Christian F. Doeller, and Caswell Barry. Deepinsight: a general framework for interpreting wide-band neural activity. *bioRxiv*, 2019.

[23] Ardi Tampuu, Tambet Matiisen, H. Freyja Ólafsdóttir, Caswell Barry, and Raul Vicente. Efficient neural decoding of self-location with a deep recurrent network. *PLOS Computational Biology*, 15:1–22, 02 2019.

[24] Jeffrey L. Elman. Finding structure in time. *Cognitive Science*, 14(2):179–211, 1990.

[25] David E. Rumelhart, Geoffrey E. Hinton, and Ronald J. Williams. Learning representations by back-propagating errors. *Nature*, 323(6088):533–536, 1986.

[26] Yann Lecun, B. Boser, J. S. Denker, D. Henderson, R. E. Howard, W. Hubbard, and L.D. Jackel. Backpropagation applied to handwritten zip code recognition. *Neural Computation*, 1(4):541–551, 1989.

[27] Andrea Banino, Caswell Barry, Benigno Uria, Charles Blundell, Timothy Lillicrap, Piotr Mirowski, Alexander Pritzel, Martin J. Chadwick, Thomas Degris, Joseph Modayil, Greg Wayne, Hubert Soyer, Fabio Viola, Brian Zhang, Ross Goroshin, Neil Rabinowitz, Razvan Pascanu, Charlie Beattie, Stig Petersen, Amir Sadik, Stephen Gaffney, Helen King, Koray Kavukcuoglu, Demis Hassabis, Raia Hadsell, and Dharshan Kumaran. Vector-based navigation using grid-like representations in artificial agents. *Nature*, 557(7705):429–433, 2018.

[28] Christopher J. Cueva and Xue-Xin Wei. Emergence of grid-like representations by training recurrent neural networks to perform spatial localization. In *International Conference on Learning Representations*, 2018.

[29] John O’Keefe. Place units in the hippocampus of the freely moving rat. *Experimental Neurology*, 51(1):78–109, 1976.

[30] Carina Curto and Vladimir Itskov. Cell groups reveal structure of stimulus space. *PLOS Computational Biology*, 4:1–13, 10 2008.

[31] Chad Giusti, Eva Pastalkova, Carina Curto, and Vladimir Itskov. Clique topology reveals intrinsic geometric structure in neural correlations. *Proceedings of the National Academy of Sciences*, 112(44):13455–13460, 2015.

[32] Miroslav Andjelković, Bosiljka Tadić, and Roderick Melnik. The topology of higher-order complexes associated with brain hubs in human connectomes. *Scientific Reports*, 10(1):17320, 2020.

[33] Rishidev Chaudhuri, Berk Gercek, Biraj Pandey, Adrien Peyrache, and Ila Fiete. The intrinsic attractor manifold and population dynamics of a canonical cognitive circuit across waking and sleep. *Nature Neuroscience*, 22(9):1512–1520, 2019.

[34] Jacob Billings, Manish Saggar, Jaroslav Hlinka, Shella Keilholz, and Giovanni Petri. Simplicial and topological descriptions of human brain dynamics. *Network Neuroscience*, 5(2):549–568, 06 2021.

[35] Mustafa Hajij, Ghada Zamzmi, Theodore Papamarkou, Vasileios Maroulas, and Xuanting Cai. Simplicial complex representation learning. *Machine Learning on Graphs (MLoG) Workshop at 15th ACM International WSD Conference*, 2022.

[36] Maosheng Yang, Elvin Isufi, and Geert Leus. Simplicial convolutional neural networks. In *ICASSP 2022 - 2022 IEEE International Conference on Acoustics, Speech and Signal Processing (ICASSP)*, pages 8847–8851, 2022.

[37] Stefania Ebli, Michaël Defferrard, and Gard Spreemann. Simplicial neural networks, 2020.

[38] Cristian Bodnar, Fabrizio Frasca, Yuguang Wang, Nina Otter, Guido F Montufar, Pietro Lió, and Michael Bronstein. Weisfeiler and lehman go topological: Message passing simplicial networks. In Marina Meila and Tong Zhang, editors, *Proceedings of the 38th International Conference on Machine Learning*, volume 139 of *Proceedings of Machine Learning Research*, pages 1026–1037. PMLR, 18–24 Jul 2021.

[39] Jeffrey S. Taube. Head direction cells and the neurophysiological basis for a sense of direction. *Progress in Neurobiology*, 55(3):225–256, 1998.

[40] Matjaž Kukar and Igor Kononenko. Cost-sensitive learning with neural networks. In *ECAI*, 1998.

[41] Klara Gerlei, Jessica Passlack, Ian Hawes, Brianna Vandrey, Holly Stevens, Ioannis Papastathopoulos, and Matthew F. Nolan. Grid cells are modulated by local head direction. *Nature Communications*, 11(1):4228, 2020.

[42] Martin Stemmler, Alexander Mathis, and Andreas V. M. Herz. Connecting multiple spatial scales to decode the population activity of grid cells. *Science Advances*, 1(11):e1500816, 2015.

[43] Demis Hassabis, Dharshan Kumaran, Christopher Summerfield, and Matthew Botvinick. Neuroscience-inspired artificial intelligence. *Neuron*, 95:245–258, 07 2017.

[44] Nitish Srivastava, Geoffrey Hinton, Alex Krizhevsky, Ilya Sutskever, and Ruslan Salakhutdinov. Dropout: A simple way to prevent neural networks from overfitting. *Journal of Machine Learning Research*, 15(56):1929–1958, 2014.

[45] Ephy R. Love, Benjamin Filippenko, Vasileios Maroulas, and Gunnar Carlsson. Topological deep learning. 2021.

[46] Vernon J Lawhern, Amelia J Solon, Nicholas R Waytowich, Stephen M Gordon, Chou P Hung, and Brent J Lance. EEGNet: a compact convolutional neural network for EEG-based brain–computer interfaces. *Journal of Neural Engineering*, 15(5):056013, jul 2018.

[47] Artur Gramacki and Jarosław Gramacki. A deep learning framework for epileptic seizure detection based on neonatal eeg signals. *Scientific Reports*, 12(1):13010, 2022.

[48] Andrew Marchese and Vasileios Maroulas. Topological learning for acoustic signal identification. In *2016 19th International Conference on Information Fusion (FUSION)*, pages 1377–1381, 2016.

[49] Theodore Papamarkou, Farzana Nasrin, Austin Lawson, Na Gong, Orlando Rios, and Vasileios Maroulas. A random persistence diagram generator. *Statistics and Computing*, 32(5), oct 2022.

[50] Vasileios Maroulas, Farzana Nasrin, and Christopher Oballe. A bayesian framework for persistent homology. *SIAM Journal on Mathematics of Data Science*, 2(1):48–74, 2020.

[51] Allen Hatcher. *Algebraic Topology*. Cambridge University Press, Cambridge, 2002.

[52] Sepp Hochreiter and Jürgen Schmidhuber. Long Short-Term Memory. *Neural Computation*, 9(8):1735–1780, 11 1997.

# Appendices

## Appendix A Proof of Proposition 1

Let  $f \in \{1, 2, \dots, F\}$  and  $\ell \in \{1, 2, \dots, L\}$  be arbitrary. Fix  $k = 0$ . Then because  $B_0 = 0 \in \mathbb{R}^{N_0 \times N_0}$ , we have

$$H_0^f(\ell) = W_0^{f,0}(\ell)I + \sum_{i=1}^D W_i^{f,0}(\ell)(B_1 B_1^T)^i, \quad (17)$$

where  $\{W_i^{f,0}(\ell)\}_{i=0}^D$  are filter parameters. Thus, the 0-dimensional component of an arbitrary filter in an arbitrary simplicial convolutional layer contains  $D + 1$  parameters. Similarly, for fixed  $k = K$ , we have

$$H_K^f(\ell) = W_0^{f,K}(\ell)I + \sum_{i=1}^D W_i^{f,K}(\ell)(B_K^T B_K)^i. \quad (18)$$

Therefore, the  $K$ -dimensional component of an arbitrary filter in an arbitrary simplicial convolutional layer also contains  $D + 1$  parameters. Now, for an intermediate dimension  $k \in \{1, 2, \dots, K - 1\}$ , a filter is defined

$$H_k^f(\ell) = W_0^{f,k}(\ell)I + \sum_{i=1}^D W_i^{f,k}(\ell)(B_k^T B_k)^i + \sum_{i=1}^D W_{i+D}^{f,k}(\ell)(B_{k+1} B_{k+1}^T)^i, \quad (19)$$

which contains  $2D + 1$  parameters  $\{W_i^{f,k}(\ell)\}_{i=0}^{2D}$ . For an arbitrary filter, there are  $K - 1$  such components (one for each dimension  $k \in \{1, 2, \dots, K - 1\}$ ). Hence, for a single filter, the total number of parameters for all intermediate  $k$ -dimensional components combined is  $(K - 1)(2D + 1)$ . Adding this sum to the number of parameters for  $k = 0$  and  $k = K$ , we see that one filter contains  $2(D + 1) + (K - 1)(2D + 1)$  parameters. Finally, because this holds for any filter in any layer, we multiply by the number of filters and the number of layers giving us  $F[2(D + 1) + (K - 1)(2D + 1)]L$  total simplicial convolutional parameters.

## Appendix B Hyperparameter Tuning

Below, we outline the different hyperparameters used throughout tuning for the results included in the main paper. For all hyperparameter tuning, we used a manual trial-and-error search method. These hyperparameters and corresponding ranges are outlined in Tables 2 and 3. Once the trial-and-error search method identified a hyperparameter value that produced the best results, we then conducted remaining trials with that value.

**HD decoding hyperparameters.** The training and test data was constructed from 20 minutes of a 38 minute session of open foraging using  $t_{bin} = 100\text{ms}$ . The first 25% of the data was used for testing data and the last 75% of the data was used for training. Ground truth labels were computed by taking the circular mean of recorded head directions within each time bin. During construction of the functional simplicial complex, the maximum dimension of simplices was bounded at  $k = 2$ . This bound was chosen due to the computational cost associated to including higher dimensional complexes. Framework hyperparameters were manually tuned within a pre-selected range to minimize CAT.

Once the best hyperparameters were identified for each of the four networks, we ran ten different trials with the ascribed hyperparameters, which can be found in Table 1, and identified the trial that resulted in the lowest CAT. When confronted with a tie, we chose the trial that had the least MAE from equation 1.

**Grid cell decoding hyperparameters.** We use 10 total minutes of recorded neural activity and ground truth position with bin sizes of  $t_{bin} = 100\text{ms}$ . The first 20% of the data was used for testing data, and the last 80% of the data was used for training. Ground truth position is computed as an average of observed positions within a time bin. We employ 2 simplicial convolutional layers of degree 2, each consisting of 3 filters and using ReLU as the nonlinear activation function. The features extracted from the simplicial convolutional layers are then fed to a RNN with 3 blocks using a hidden dimension of size 50. The network trained for 50 epochs on a batch size of 16 with learning rate 0.001. Similar to the HD decoding task, framework hyperparameters were manually tuned within a pre-selected range to minimize AED.

	FFNN	SCNN	RNN	SCRNN
Batch Size	16	8	8	32
Max Conv. Dim.	N/A	1	N/A	1
SC Layers	N/A	1	N/A	2
N_filters	N/A	3	N/A	3
Degree	N/A	2	N/A	2
NN Layers	3	3	2	2
NN Width	128, 128, 64	128, 128, 64	N/A	N/A
Hidden Size	N/A	N/A	100	50
Test MAE	12.75	11.56	11.26	10.96
Test AAE	16.85	15.43	14.49	14.11
CAT	70	94	9	6

Table 1: A table comparing the different networks based on their trial with the lowest catastrophic error. All trials were executed with 100 epochs, threshold 30, learning rate 0.001, and dropout rate 0.2. For the NN Width, the three values denote the size of each NN Layer.

Decoding Method	Hyperparameter	Range
FFNN	Epochs	100
	Batch Size	4, 8, 16, 32
	Learning Rate	0.001
	NN Layers	1, 2, 3
	Layer Width	64, 128, 256
	Activation Function	ReLU
SCNN	Intervals per Sample	1, 2, 3, 4
	Epochs	100
	Batch Size	8, 16, 32
	Learning Rate	0.001
	Dropout	0.2, 0.3
	SC Layers	1, 2
	Number of Filters	3
	NN Layers	1, 2, 3
	Layer Width	64, 128
	Activation Function	ReLU
RNN	Epochs	100
	Batch Size	8, 16, 32
	Learning Rate	0.001
	Dropout	0.2, 0.3
	NN Layers	1, 2
	Hidden Size	25, 30, 40, 50, 75, 100
	Activation Function	ReLU
SCRNN	Epochs	50, 100
	Sequence Length	3, 5, 8
	Threshold	5, 10, 30
	Batch Size	8, 16, 32
	Learning Rate	0.001
	Dropout	0.2, 0.3
	SC Layers	1, 2
	Number of Filters	3
	NN Layers	1, 2
	Hidden Size	50
	Activation Function	ReLU

Table 2: Search values used for hyperparameter tuning. All hyperparameter search tests were conducted with 15 minutes of training data and 5 minutes of testing data.

Decoding Method	Hyperparameter	Range
SCRNN	Test % of Data	20%
	Epochs	50
	Sequence Length	3, 5, 8
	Threshold	1, 10, 20
	Batch Size	8, 16, 32, 64
	Learning Rate	0.0001, 0.001
	Dropout	0.2, 0.3
	SC Layers	1, 2, 3, 5
	Number of Filters	2, 3, 5
	NN Layers	1, 3, 5
	Hidden Size	25, 40, 50, 75, 100, 200
	Activation Function	ReLU

Table 3: A table of hyperparameter values used during hyperparameter tuning for the grid cell decoding task. Following the same procedure as was done for the HD application, we used a manual trial-and-error search method to identify optimal hyperparameters that minimized AED.

## Appendix C Analysis of Different Train/Test Splits

In this section, we show results for the HD decoding task with two different training and testing data splits: one with 50% training, 50% testing (Figure 6) and another with 25% training, 75% testing (Figure 7). Following the same manual hyperparameter tuning procedure mentioned in Supplementary Section B, we tuned the FFNN, SCNN, SCRNN, and RNN to minimize CAT. For both splits, we observe the SCRNN provides the best results.

**Training: 10 minutes, Testing: 10 minutes** The results below correspond to 10 minutes of training data and 10 minutes of testing data. Note, the SCRNN has the lowest MAE, AAE, and CAT across all architectures.

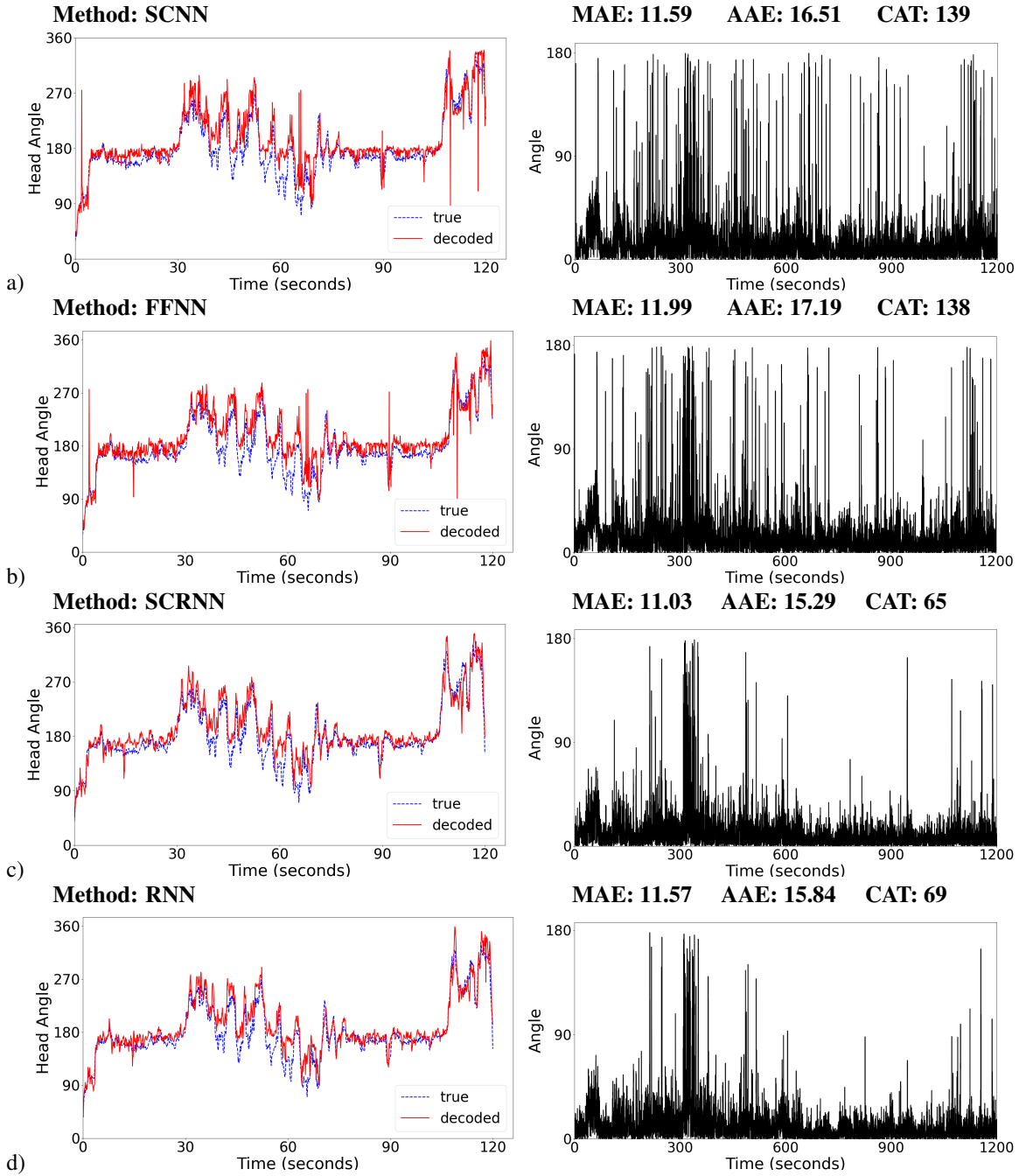


Figure 6: Plots depicting the true head angle and the predicted head angle for the first two minutes with the catastrophic error for each time bin for four different networks, a) SCNN, b) FFNN, c) SCRNN, and d) RNN.

**Training: 5 minutes, Testing: 15 minutes** Next, the results below correspond to 5 minutes of training data and 15 minutes of testing data. Again, the SCRNN has the lowest MAE, AAE, and CAT across all architectures.

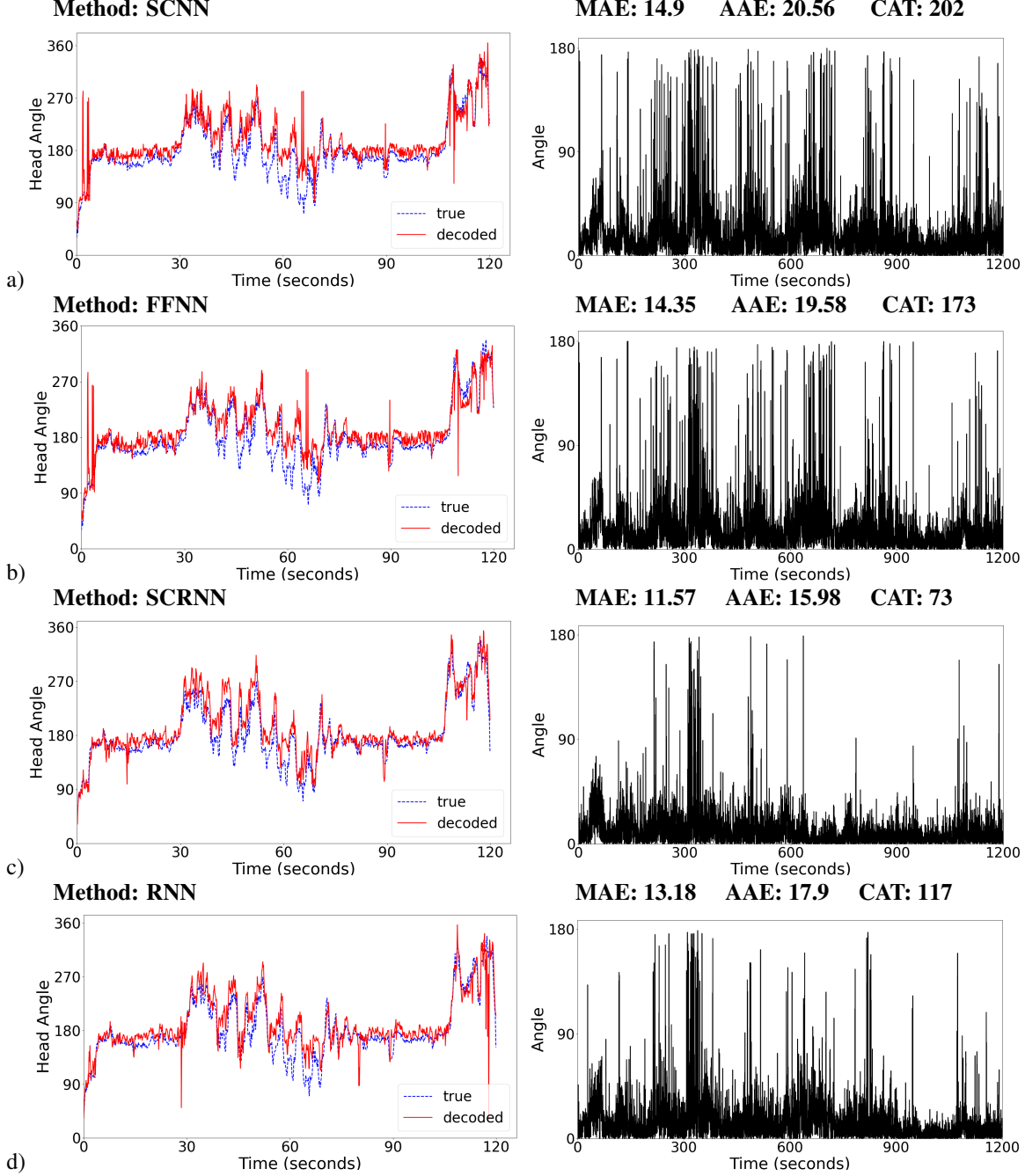


Figure 7: Plots depicting the true head angle and the predicted head angle for the first two minutes with the catastrophic error for each time bin for four different networks, a) SCNN, b) FFNN, c) SCRNN, and d) RNN.

## Appendix D Neural Data

In this section, we include visualizations of the neural activity in the form of raster plots. The spike trains of all 22 HD cells used in the HD decoding task are shown in Figure 8. Note how cells can differ in firing pattern. The pre-processing procedure of our framework accounts for this in the binarization step by thresholding row-wise, meaning a neuron's activity is compared to itself. Otherwise, neurons that fire more frequently would lead to the complete zeroing out of activity of neurons that, by comparison, rarely fired.

Figure 9 shows the spike trains from a single module used in the grid cell decoding task. This module consists of 166 neurons. The other two modules (not shown) used in the grid cell decoding task consist of 167 and 149 grid cells. The increased number of neurons compared to the HD system is necessary to encode a two-dimensional variable and makes the grid cell decoding task more complex.

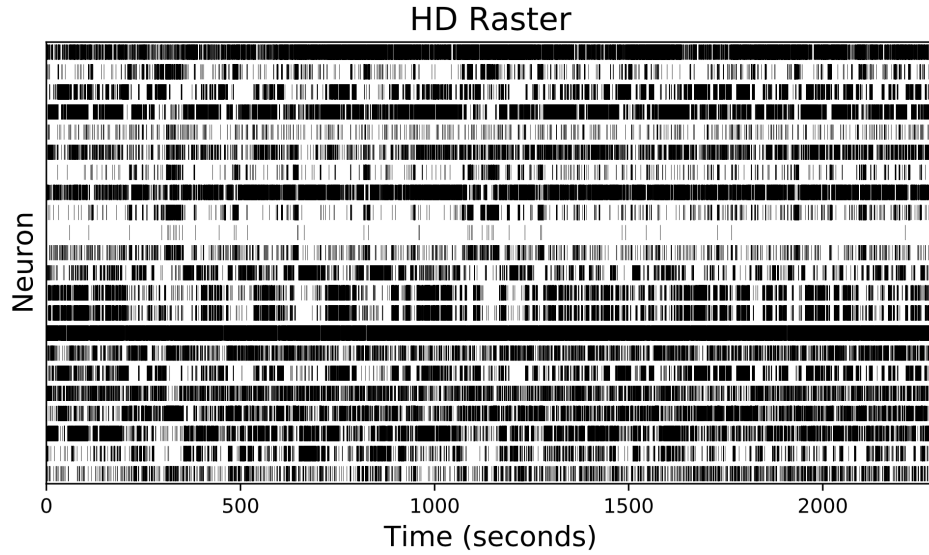


Figure 8: A raster plot showing the HD neural activity from ‘Mouse28-140313’ in the source data [17]. The HD system includes 22 neurons recorded over a 38 minute period while the mouse foraged in an open environment.

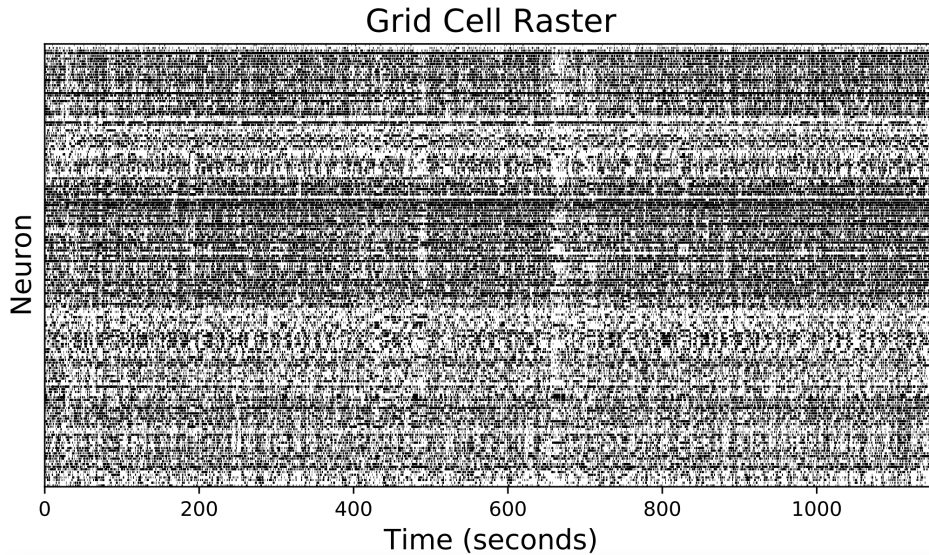


Figure 9: A raster plot showing the neural activity from a single module of 166 grid cells recorded over a 19 minute period while the rat foraged in an open  $1.5 \times 1.5$  meter environment. The data is labeled R1 day 1 in the source data [1].